# MutL traps MutS at a DNA mismatch

Ruoyi Qiu[a], Miho Sakato[b], Elizabeth J. Sacho[a], Hunter Wilkins[c], Xingdong Zhang[d], Paul Modrich[d,e], Manju M. Hingorani[b], Dorothy A. Erie[c,f,1], and Keith R. Weninger[a,1]

[a]Department of Physics, North Carolina State University, Raleigh, NC 27695; [b]Molecular Biology and Biochemistry Department, Wesleyan University, Middletown, CT 06459; [c]Department of Chemistry, University of North Carolina at Chapel Hill, Chapel Hill, NC 27599; [d]Department of Biochemistry, Duke University Medical Center, Durham, NC 27710; [e]Howard Hughes Medical Institute, Duke University Medical Center, Durham, NC 27710; and [f]Curriculum in Applied Sciences and Engineering, University of North Carolina at Chapel Hill, Chapel Hill, NC 27599

Edited by John A. Tainer, Scripps Research Institute, La Jolla, CA, and accepted by the Editorial Board July 21, 2015 (received for review March 20, 2015)

**DNA mismatch repair (MMR) identifies and corrects errors made during replication. In all organisms except those expressing MutH, interactions between a DNA mismatch, MutS, MutL, and the replication processivity factor (β-clamp or PCNA) activate the latent MutL endonuclease to nick the error-containing daughter strand. This nick provides an entry point for downstream repair proteins. Despite the well-established significance of strand-specific nicking in MMR, the mechanism(s) by which MutS and MutL assemble on mismatch DNA to allow the subsequent activation of MutL's endonuclease activity by β-clamp/PCNA remains elusive. In both prokaryotes and eukaryotes, MutS homologs undergo conformational changes to a mobile clamp state that can move away from the mismatch. However, the function of this MutS mobile clamp is unknown. Furthermore, whether the interaction with MutL leads to a mobile MutS–MutL complex or a mismatch-localized complex is hotly debated. We used single molecule FRET to determine that *Thermus aquaticus* MutL traps MutS at a DNA mismatch after recognition but before its conversion to a sliding clamp. Rather than a clamp, a conformationally dynamic protein assembly typically containing more MutL than MutS is formed at the mismatch. This complex provides a local marker where interaction with β-clamp/PCNA could distinguish parent/daughter strand identity. Our finding that MutL fundamentally changes MutS actions following mismatch detection reframes current thinking on MMR signaling processes critical for genomic stability.**

DNA mismatch repair | MutS | MutL | FRET

The DNA mismatch repair (MMR) system employs several proteins to locate and correct DNA replication errors that escape polymerase proofreading. Mutations in these proteins contribute to MMR dysfunction that is associated with carcinogenesis, such as Lynch syndrome and other diseases associated with high mutator phenotypes (1, 2). In all organisms, MMR is initiated by binding of MutS homologs to a base–base mismatch or an insertion/deletion loop (IDL), followed by ATP-dependent recruitment of MutL homologs to begin the process of repair (3, 4). Following MutL recruitment, a key event is the introduction of a nick that directs excision and resynthesis of the nascent DNA strand containing the error (5–7).

In methyl-directed MMR, which occurs in *Escherichia coli*, the mismatch- and ATP-dependent MutS–MutL–DNA complex activates the protein MutH to nick transiently unmethylated d(GATC) sequences in the daughter strand. Notably, however, MutH is not widely conserved in prokaryotes and does not exist in eukaryotes. Recent in vitro studies of eukaryotic MMR indicate that in these MutH-free organisms, detection of a mismatch by MutS or MutSα [MutS(α)] licenses MutL(α) to interact with the processivity factor (β-clamp/PCNA), which in turn activates the latent endonuclease activity of MutL(α) to incise the daughter DNA strand on both the 3′ and 5′ sides of the error (8–11). The interaction between MutL and the β-clamp (or between MutLα and PCNA) provides the strand discrimination signal because the β-clamp (or PCNA) is loaded asymmetrically at the replication fork or at a nick in DNA (10, 12).

The importance of the nicking activity of MutL homologs is highlighted by the observation that mutations that impair yeast MutLα endonuclease activity cause a significant mutator phenotype and genomic instability (11, 13, 14). Despite the well-established significance of strand-specific nicking in MMR, the mechanism(s) by which MutS and MutL assemble on mismatched DNA to allow subsequent activation of MutL endonuclease activity by β-clamp/PCNA remains elusive. There is general agreement that in both prokaryotes and eukaryotes, after binding a mismatch MutS or MutSα can undergo conformational changes to a mobile clamp state that can move away from the mismatch (6, 15). What happens after this step is mired in controversy. Several disparate models for MutS(α)–MutL(α) mismatch complex formation and the subsequent signaling of repair have been proposed (e.g., see refs. 6, 7, 15–21). One prominent model in the field has MutL(α) joining MutS(α) to form MutS(α)–MutL(α) sliding clamps that diffuse along the DNA to interact with the strand-discrimination signal (β-clamp/PCNA or MutH) (16). Other models include trapping of MutS(α) clamps near the mismatch by MutL(α) followed by DNA looping or, alternately, MutS(α)-induced polymerization of MutL(α) along the DNA to reach the strand-discrimination signal (6, 7, 15, 18, 22). Some degree of localization to the mismatch is suggested by in vitro studies of eukaryotic MMR proteins, indicating that although MutLα can introduce nicks across long stretches of DNA, they occur preferentially in the vicinity of the mismatch (9, 11, 12).

In this study, we have used single molecule fluorescence to demonstrate that in the case of *Thermus aquaticus* (a MutH-free organism), MutL traps MutS at the mismatch after its ATP-induced

## Significance

**DNA mismatch repair is the process by which errors generated during DNA replication are corrected. Mutations in the proteins that initiate mismatch repair, MutS and MutL, are associated with greater than 80% of hereditary nonpolyposis colorectal cancer (HNPCC) and many sporadic cancers. The assembly of MutS and MutL at a mismatch is an essential step for initiating repair; however, the nature of these interactions is poorly understood. Here, we have discovered that MutL fundamentally changes the properties of mismatch-bound MutS by preventing it from sliding away from the mismatch, which it normally does when isolated. This finding suggests a mechanism for localizing the activity of repair proteins near the mismatch.**

Author contributions: R.Q., M.M.H., D.A.E., and K.R.W. designed research; R.Q., M.S., E.J.S., H.W., and D.A.E. performed research; R.Q., M.S., H.W., X.Z., P.M., M.M.H., and K.R.W. contributed new reagents/analytic tools; R.Q., M.S., E.J.S., M.M.H., D.A.E., and K.R.W. analyzed data; and P.M., M.M.H., D.A.E., and K.R.W. wrote the paper.

The authors declare no conflict of interest.

This article is a PNAS Direct Submission. J.A.T. is a guest editor invited by the Editorial Board.

[1]To whom correspondence may be addressed. Email: keith_weninger@ncsu.edu or derie@unc.edu.

This article contains supporting information online at www.pnas.org/lookup/suppl/doi:10.1073/pnas.1505655112/-/DCSupplemental.

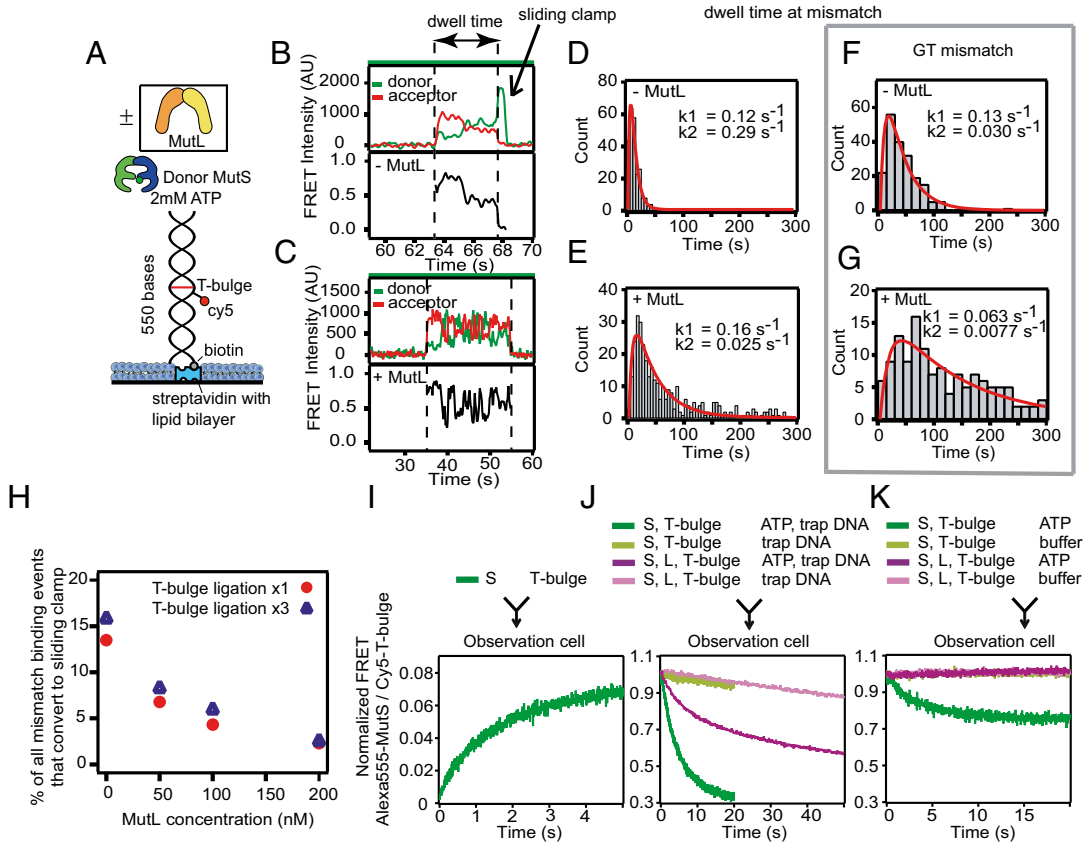


**Fig. 1.** MutL extends the bound time of MutS at a DNA mismatch with ATP. (*A*) Experimental scheme: 2 mM ATP, 10 nM Alexa 555–MutS (donor), Cy5–T-bulge DNA (acceptor), and 200 nM unlabeled MutL (when present). Example time traces of donor and acceptor emission under 532-nm illumination and calculated FRET in the absence (*B*) and presence (*C*) of MutL. The dashed lines denote dwell times at the mismatch for these events. Histograms of total mismatch dwell times for hundreds of individual MutS-mismatch binding events with exactly one donor and one acceptor in the absence (*D*) or presence (*E*) of MutL were fit (red lines) with indicated rates for a two-step transition (*SI Materials and Methods*). Similar measurements of GT mismatched DNA in the absence (*F*) or presence (*G*) of MutL. In *B* (and Fig. 4*B*) the sliding clamp state (indicated) characterized by FRET = 0 is verified by (*i*) acceptor emission under red laser illumination at the end of the data acquisition, and (*ii*) the duration of the FRET = 0 state is shorter than typical donor bleaching but is consistent with expected dwell time of a sliding clamp MutS on unblocked DNA (as described in detail in ref. 21.) In *H*, MutS sliding clamp formation correlates inversely with MutL concentration. In buffer with 2 mM ATP, about 80% of the MutS binding events are identical to those with 2 mM ADP (i.e., FRET value of 0.68, lifetime of 2.7 s and direct dissociation from the mismatch without sliding). In the remaining 20% binding events, FRET transitions were observed with or without MutL. Of these FRET transitioning events, 80% resulted in MutS conversion to sliding clamps in the absence of MutL (~15% of total MutS binding events). As MutL concentration was raised, the fraction of transitioning FRET events in which MutS converted to sliding clamps decreased dramatically. With 200 nM MutL in the reaction, only about 15% of the dynamic FRET events resulted in sliding clamps (~3% of total MutS binding events). These populations were not affected by preexisting nicks in DNA, because the results were the same for substrates with more (1× ligase-treated DNA; circle) or fewer nicks (3× ligase-treated DNA; triangle). See more details in Fig. S3 and *SI Materials and Methods*. (*I–K*) Ensemble studies confirm MutL-induced stabilization of ATP-bound MutS at a mismatch. FRET between Alexa 555–MutS and Cy5–T bulge was used to monitor the effects of ATP and MutL on MutS interactions with mismatched DNA. (*I*) Stopped-flow trace showing increase in FRET as Alexa 555–MutS (0.13 μM) binds Cy5–T bulge at 0.6 $s^{-1}$ at 40 °C (apparent $k_{on}$ = 4.6 × $10^6$ $M^{-1}{\cdot}s^{-1}$); this rate constant is consistent with previous bulk kinetic measurements of 3–6 × $10^6$ $M^{-1}{\cdot}s^{-1}$ using 5-carboxytetramethylrhodamine (TAMRA) or 2-aminopurine labeled DNA (28, 38). (*J*) Stopped flow traces of Alexa 555–MutS and Cy5–T bulge mixed with excess unlabeled trap T-bulge DNA show slow FRET decrease, indicating release of MutS from the mismatch at 0.01 $s^{-1}$ in the absence of ATP (comparable to the previously reported rate of 0.05 $s^{-1}$ with TAMRA-labeled DNA) (28), irrespective of MutL (light green, pink traces). ATP binding to MutS stimulates its release from the mismatch as a sliding clamp at a ~20-fold faster rate of 0.2 $s^{-1}$ (dark green trace), similar to that reported from single molecule measurements with the same assay system (21) and ensemble measurements with TAMRA-labeled DNA (28). But addition of MutL stabilizes the complex such that only a fraction of ATP-bound MutS (~1/3) is released as a sliding clamp at 0.2 $s^{-1}$, whereas most of it is retained at the T-bulge and dissociates 10-fold slower at 0.02 $s^{-1}$ (purple trace). (*K*) The same experiment performed in the absence of trap DNA (i.e., free MutS can rebind Cy5–T bulge) confirms that MutL stabilizes the MutS–ATP–T-bulge complex, as there is no net decrease in FRET over time (purple trace) in contrast with ATP-induced sliding of MutS off the mismatch at 0.3 $s^{-1}$ in the absence of MutL (dark green trace; the amplitude change is smaller than in the reaction with trap DNA (*J*) due to a fraction of MutS rebinding Cy5–T bulge following ATP hydrolysis).

activation but before its conversion into a sliding clamp. The resulting MutS–MutL mismatch complex typically contains more MutL than MutS, with one or two MutS dimers and up to four MutL dimers. MutS exists in a conformationally dynamic state within these complexes, which may be relevant for subsequent steps in MMR. In contrast to a mobile MutS–MutL complex, localization of MutS–MutL at the mismatch can restrict β-clamp/PCNA-activated MutL nicking to the vicinity of the mismatch, thereby enhancing MMR efficiency and limiting excessive excision and resynthesis that can destabilize the genome.

## Results and Discussion

**MutL Lengthens the Dwell Time of MutS at a DNA Mismatch.** We recently used single molecule fluorescence resonance energy transfer (FRET) between donor fluorophore-labeled *T. aquaticus* (Taq) MutS protein and DNA with an acceptor dye located 9 bp from a T bulge to monitor the interaction of MutS with a mismatch in the presence of ADP or ATP (21). Results from that study revealed that in the presence of ATP, 20% of the mismatch-bound MutS proteins convert into sliding clamps (as reported by transition to FRET 0; Fig. 1 *A* and *B*), whereas the other 80%

exhibit simple mismatch binding and dissociation with the same kinetics as seen in the presence of ADP, presumably having undergone ATP hydrolysis prior to mismatch binding (21).

In this study, we examined the effects of MutL on MutS–DNA interactions under different nucleotide conditions. Addition of MutL does not alter the behavior of MutS on mismatched DNA in the presence of ADP, nor of the 80% of MutS in the presence of ATP that behaves the same as with ADP (Fig. S1). In contrast, MutL dramatically alters the behavior of 20% of MutS in the presence of ATP (Fig. 1*C*), which is the same fraction of MutS that forms ATP-bound sliding clamps in the absence of MutL (21). Decreasing MutL concentration decreases the fraction of MutS proteins that show these altered properties, confirming a MutL-specific effect (Fig. 1*H*). For this subset, (*i*) MutL increases the residence time of MutS at the mismatch by ~10-fold, from ~5 s to 40 s (Fig. 1 *D* and *E*); (*ii*) MutS rarely exhibits a FRET of 0 before dissociation (or photobleaching), indicating that the MutL-stabilized MutS-mismatch complexes do not form sliding clamps that move away from the mismatch before dissociation (Fig. 1*C*); and (*iii*) MutL alters the conformations and dynamics of MutS at the mismatch (discussed later). Notably, experiments with DNA containing a GT mismatch demonstrate that MutL also increases the overall lifetime of ATP-bound MutS at a GT mismatch by ~10-fold (Fig. 1 *F* and *G*), from tens of seconds to hundreds of seconds, indicating that these findings are not limited to a T bulge (*SI Materials and Methods* and Fig. S1 *A–D* for details on the MutS–GT DNA complex and *SI Materials and Methods* and Fig. S1*E* for additional controls). Finally, consistent with these single molecule results, stopped-flow ensemble experiments monitoring FRET between MutS and T-bulge DNA at 40 °C also show that MutL increases the residence time of ATP-bound MutS at a mismatch by ~10-fold (Fig. 1 *I–K* and *SI Materials and Methods*).

**MutL Prevents Loading of Multiple MutS on End-Blocked, Mismatch-Containing DNA.** Previous studies, including ours, have shown that ATP-dependent conversion of MutS into a sliding clamp frees up the mismatch site and allows loading of multiple MutS proteins, which get trapped on end-blocked DNA (5, 17, 20, 21). The observation that MutL stabilizes MutS at a mismatch predicts that MutS loading onto end-blocked DNA should be reduced in the presence of MutL. Monitoring the photobleaching of fluorescently labeled MutS on an end-blocked T-bulge substrate in the presence of ATP reveals that without MutL, up to eight MutS dimers can be loaded per DNA with lifetimes greater than 600 s (Fig. 2 *A–C*) (20, 21). In contrast, addition of MutL greatly reduces accumulation of MutS sliding clamps, such that most DNAs are bound by only one or two MutS dimers (Fig. 2 *D* and *E*). In addition, in the absence of MutL, zero FRET (Fig. 2*B*) indicates MutS sliding clamps move away from the mismatch, whereas with MutL present, nonzero FRET (Fig. 2*D*) indicates at least one MutS remains near the mismatch. These results taken together with the FRET data described above (Fig. 1) indicate that MutL traps one or two MutS dimers at or near the mismatch.

**Stoichiometry of MutS–MutL Mismatch DNA Complexes.** Because the dynamic experiments (as in Fig. 1) are limited to concentrations of ~10 nM fluorescent protein, to examine the stoichiometries of MutS–MutL-mismatch complexes in more detail, we (*i*) incubated Alexa 647-tagged MutS (10 nM or 100 nM) and Alexa 555-tagged MutL (200 nM) with biotinylated T-bulge–DNA at room temperature and 40 °C, (*ii*) crosslinked the complexes with glutaraldehyde, (*iii*) captured the crosslinked complexes on a streptavidin surface, and (*iv*) used single-molecule fluorescence photobleaching to determine the number of Alexa 647-tagged MutS and Alexa 555-tagged MutL proteins in each complex (Fig. 3 and Fig. S2 *A–D*). In all cases, formation of complexes

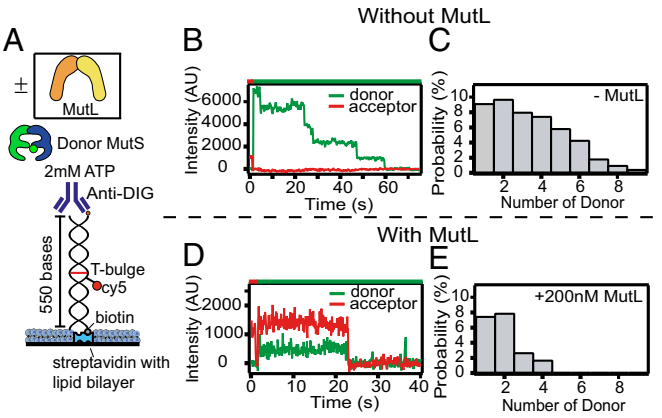


**Fig. 2.** MutL suppresses multiple MutS loading in the presence of ATP on end-blocked T-bulge DNA. (*A*) Experimental scheme as in Fig 1, except with anti-digoxin end-blocked DNA. The proteins, 10 nM Alexa 555–MutS (75% label efficiency) and 200 nM MutL, were incubated for 15 min and rinsed. Example time traces of donor and acceptor emission with laser illumination indicated at the *Top* in the absence (*B*) and presence (*D*) of MutL. Red illumination was used first to locate Cy5–T-bulge DNA followed by green illumination to excite Alexa 555–MutS. Photobleaching steps were counted to determine MutS occupancy. Multiple MutS loading occurs without MutL in solution (*C*) and is suppressed with addition of MutL (*E*). Note, the FRET value 0 in *B* indicates MutS is in a sliding clamp form, having left the mismatch, whereas nonzero FRET in *D* indicates MutS is at (or near) the DNA mismatch.

containing MutL required the presence of mismatched DNA, ATP, and MutS (Fig. S2 *E–G*), and we observed no significant population of excessively large assemblies. Most complexes contain one to two MutS dimers and two to three MutL dimers (Fig. 3*D* and Fig. S2). This number of MutS dimers is consistent with the number of dimers that we observe in our dynamic experiments with labeled MutS and unlabeled MutL (Fig. 2 *D* and *E*). In addition, the total number of proteins in the complex is similar to the number of proteins in complexes of yeast MutSα–MutLα detected by surface plasmon resonance (23). The observed excess of MutL over MutS contrasts with the proposed 1:1 stoichiometry in MutS–MutL sliding clamps (16, 24), but agrees with in vivo studies in *E. coli* and yeast, where repair foci contain more MutL than MutS proteins (18, 22), and with early DNA footprinting studies indicating complexes containing multiple MutS and MutL proteins at the mismatch (3, 25). Consistent with the latter observation, additional crosslinking experiments using unlabeled MutL, Alexa 555-tagged MutS and the Cy5–T-bulge–DNA revealed FRET in all complexes, confirming their presence near the mismatch, consistent with our dynamic experiments with uncrosslinked proteins (Fig. 2*D*). Rather than a sliding MutS–MutL clamp model, our findings suggest a model in which MutL flanks MutS at the mismatch, as first suggested by Modrich and coworkers (6, 7) and more recently by other investigators (18, 22).

**Intermediate Steps During Assembly of MutS–MutL Complexes.** Having characterized the composition of the MutS–MutL complexes at a mismatch, we next sought to elucidate the mechanism of complex formation. To this end, we examined the impact of MutL on the kinetics of MutS mismatch recognition and its subsequent conformational changes in solution, in real time (Fig. 4*A*). Our previous experiments (21) showed that conversion of MutS into a sliding clamp involves at least two steps wherein MutS first binds to the mismatch (resulting in FRET of 0.65) and then undergoes a conformational change (resulting in FRET 0.45) before forming a clamp that diffuses away from the mismatch (resulting in FRET 0) and slides off the free DNA end (resulting in loss of the donor signal) (Figs. 1*B* and 4*B*).

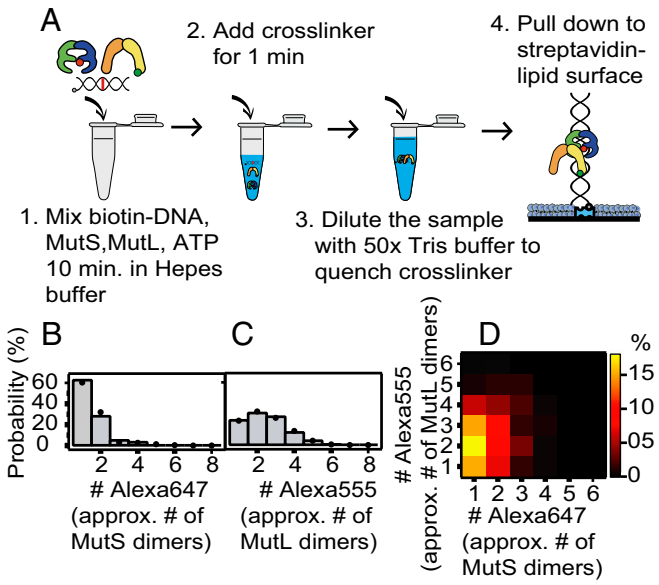


**Fig. 3.** Stoichiometry of MutS/MutL/T-bulge DNA complexes. (*A*) Experimental scheme: 10 nM Alexa 647–MutS, 200 nM Alexa 555–MutL, 5 nM biotinylated T-bulge DNA, and 2 mM ATP mixed to form complexes, followed by crosslinking, biotin-capture on the surface, and photobleaching-step counting. Photobleaching steps indicate that the distribution of MutS (*B*) and MutL (*C*) is maximal at 2 MutL and 1 MutS within a complex (*D*). The large dots in *B* and *C* are predicted dye distributions for each complex, given 50% labeling efficiencies of MutS and MutL in this experiment (*SI Materials and Methods*). Note, the number of MutS agrees in measurements with and without crosslinking (compare Figs. 2*E* and 3*B*). Atomic force microscope (AFM) imaging of crosslinked complexes yielded volumes consistent with these results (Fig. S2*D* and *SI Materials and Methods*).

As expected, MutL does not alter the FRET of the initial MutS mismatch recognition complex (0.65); however, it dramatically changes subsequent conformational transitions. The dwell-time distributions of the first FRET state (0.65) in the presence or absence of MutL exhibit clear rise and decay (Fig. 4 *D* and *G*), indicating two rate-limiting steps between FRET 0.65 and the next FRET state (26, 27) and therefore the existence of two states with a FRET of 0.65 (which we designate 0.65 and 0.65*) (Fig. 4*H*). Fitting these data (*SI Materials and Methods*) (Fig. 4 *D* and *G*, red lines) yields similar rates in the absence of MutL ($1.1 \pm 0.67\ s^{-1}$ and $0.45 \pm 0.02\ s^{-1}$) and in its presence ($0.56 \pm 0.14\ s^{-1}$ and $0.20 \pm 0.05\ s^{-1}$). Given that the rates of both transitions are slower than the estimated rate of ATP-induced ADP dissociation measured in ensemble studies (28), we propose that the first step (0.65→0.65*) requires ADP release followed by rapid ATP binding ($10^6\ M^{-1}{\cdot}s^{-1}$ and $>10^3\ s^{-1}$ at 2 mM ATP) (28, 29), and the second step (to FRET 0.45 without MutL; Fig. 4 *C* and *D*) is a conformational change of the doubly ATP-liganded state (Fig. 4*H*), consistent with previous suggestions (15, 17). Notably, although MutL does not dramatically impact the FRET levels or kinetics of the initial MutS conformational change (0.65→0.65*), it alters the subsequent conformation, which exhibits FRET 0.45 without MutL but FRET 0.3 with MutL. These results indicate that MutL interacts with MutS after the ADP–ATP exchange, as suggested by previous studies (15, 17), but before MutS transitions to FRET 0.45, demonstrating that MutL binding to MutS immediately after its ATP binding-induced conformational change traps it at the mismatch (Fig. 4*H*). This latter finding provides an explanation for the observation that yMutLα can interact with an ATPase-site mutant of yMutSα that does not form a sliding clamp (30). Interestingly, a recent study monitoring DNA bending with small angle X-ray scattering in solution (31), suggests that, for *E. coli* proteins, MutL interacts with MutS after an ATP-dependent conformational change from a bent DNA state to an unbent DNA state. If *E. coli* and Taq MMR follow the same pathway (discussed later in *Conclusions*), then extrapolating this result suggests that our FRET 0.45 state (between protein and DNA) involves unbent DNA (Fig. 4*H*) (32, 33).

In the absence of MutL, MutS in the 0.45 FRET state transitions to a sliding clamp with FRET of 0 and ultimately slides off the free DNA end (no donor fluorescence) (Fig. 4*B*). In contrast, in the presence of MutL, MutS remains at the mismatch and fluctuates rapidly between FRET of 0.3 and 0.6 before eventually dissociating directly from the mismatch (or photobleaching) without transitioning to 0 FRET (Figs. 1*C* and 4*E*). The narrowness of the FRET 0.3 and 0.6 histograms (Fig. 4*F*) confirms that MutL-stabilized MutS remains at or very near the mismatched base, because movement of MutS even a few nucleotides from the mismatch would broaden the FRET distributions. In addition, we only observe these two interconverting states (FRET 0.3 and 0.6) in the presence of MutL (Fig. 4 *F* vs. *C*), strongly suggesting that MutL is present and is influencing the conformation of MutS. To understand the nature of the rapid transitions, we also monitored intraprotein FRET between donor and acceptor fluorophore-tagged mismatch binding domains I of MutS dimers bound to unlabeled DNA (Fig. S3 *A–D*). The data show that these domains alternate between two conformational states with the same kinetics as the FRET transitions seen between MutS and the DNA (Fig. 4*F*). Taken together, these results indicate that MutL traps MutS at (or very near) the mismatch site, but that MutS mismatch binding domains remain mobile. It is notable that MutS domains I switch between conformationally mobile and static states depending on its ligand-bound form (e.g., mobile in free MutS, static in mismatch-bound MutS and then mobile again in ATP-, mismatch- and MutL-bound MutS) (21). A specific role for MutS domain I dynamics in signaling downstream events after mismatch recognition remains to be determined.

## Conclusions

In summary, by directly monitoring assembly of individual MutS–MutL complexes at DNA mismatches, we have observed initial events in the repair mechanism following mismatch recognition. The observation that MutL can trap MutS at the mismatch before it forms a sliding clamp raises the question of what function might be served by sliding clamps. It may be the means by which MutS clears the mismatch site if MutL does not arrive in a timely manner to initiate repair. Our study also does not rule out the possibility that mobile MutS–MutL signaling complexes may form and complement the functions of stationary MutS–MutL mismatch complexes in DNA repair, e.g., for long-range search of a strand-discrimination signal when one is not available near the mismatch (5, 16). In MutH-dependent methyl-directed MMR (as in *E. coli*), localized assembly of MutS–MutL at the mismatch alone cannot account for orientation-dependent loading of the appropriate 5′-to-3′ or 3′-to-5′ excision system at the nick made by MutH at a d(GATC) site (34), because the mismatch can be up to a kilobase from the break (35) and the helicase loading process must involve signaling along the helix contour. The apparent requirement for mobile MutS–MutL complexes in methyl-directed repair may reflect fundamental differences from MutH-independent repair, such as in Taq and eukaryotes. In particular, early steps in methyl-directed repair are β/PCNA clamp-independent and the MutL homolog lacks endonuclease activity (34), whereas, in MutH-independent repair, MutL has latent endonuclease activity that is activated by β/PCNA at an early step. In the latter system, interactions between β/PCNA clamps, which are loaded onto primer-template DNA junctions in a specific orientation, and MutS–MutL complexes trapped at the mismatch site could direct MutL nicking

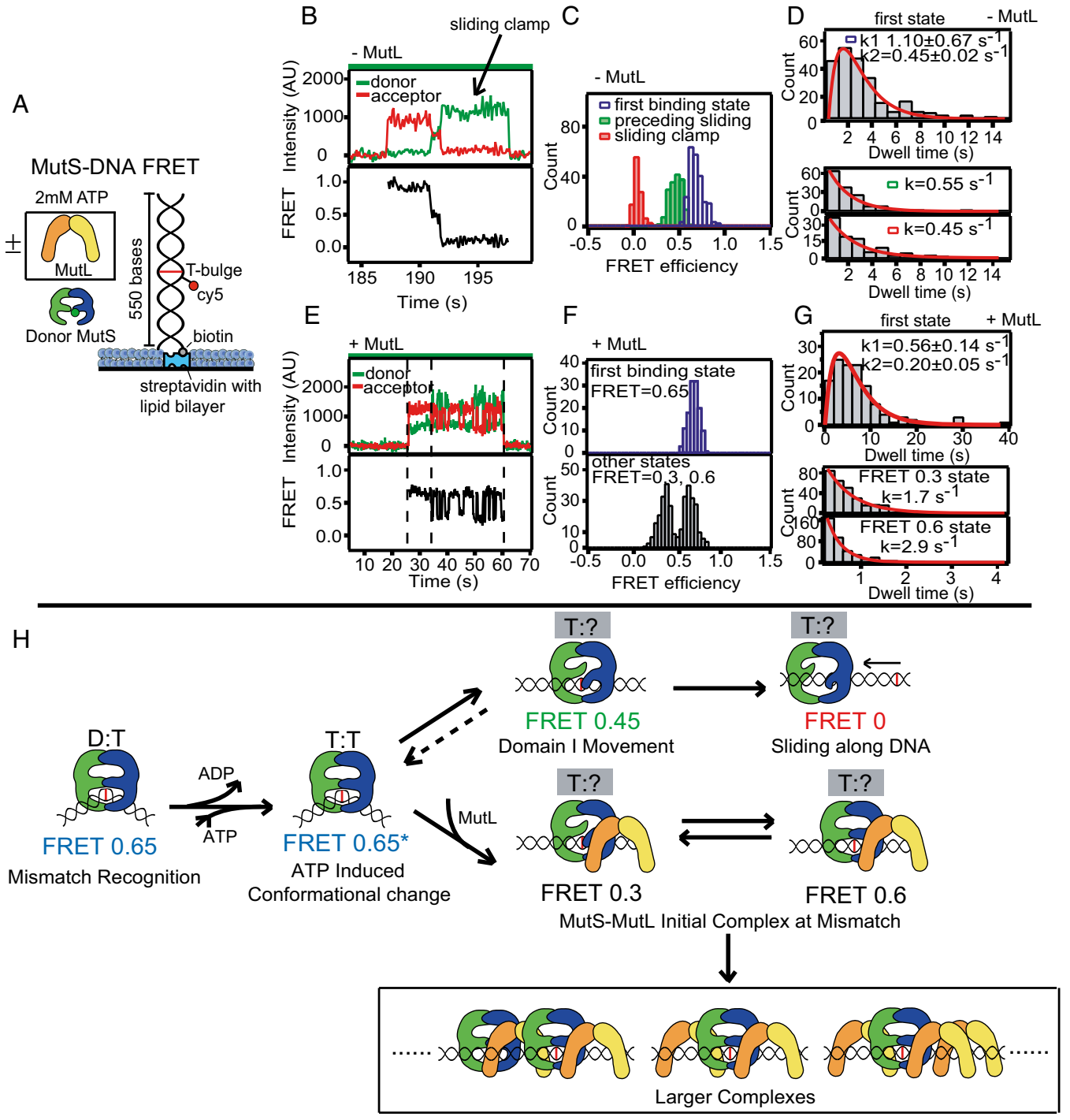


**Fig. 4.** MutL alters the kinetics of MutS mismatch recognition and subsequent conformational changes. (*A*) Experimental scheme: 2 mM ATP, 10 nM Alexa 555–MutS, Cy5–T-bulge DNA, and 200 nM unlabeled MutL (when present). Example time traces of donor and acceptor emission and calculated FRET in the absence (*B*) and presence (*E*) of MutL for events with transitions. FRET histograms for binding events with exactly one donor and one acceptor and with FRET transitions reveal three states in the absence of MutL (*C*) with dwell time distributions fit (red line) by a two-step model for the first state (*D*, *Top* show rates $1.1 \pm 0.67\ s^{-1}$ and $0.45 \pm 0.02\ s^{-1}$, where ± indicates SE of two independent replicates) and a one-step model for the middle state and last state (*D*, *Middle* and *Lower*). In the presence of MutL, FRET histograms for the first state (*F*, *Top*) reveal a narrow peak, but the dwell time distributions (*G*, *Top*) still require a fit (red line) with two steps (rates $0.56 \pm 0.14\ s^{-1}$ and $0.20 \pm 0.05\ s^{-1}$, where ± indicates SE of two independent replicates). Histograms of the subsequent FRET states show two nonzero peaks (*F*, *Lower*), and the dwell time distributions fit well (red line) with a one-step model (*G*, *Middle* and *Lower*). Numbers within panels report rates obtained from the fits. (*H*) A model derived from the results (MutL: yellow/tan; MutS: green/blue). The proposed FRET states, MutS nucleotide states (D, ADP and T, ATP *Above* MutS) as well as MutS and DNA conformations are indicated. Later nucleotide states of MutS that are not yet precisely determined are marked by gray shading.

activity to the nascent strand in the vicinity of the mismatch. This constraint would in turn limit the extent of strand excision and resynthesis and increase the efficiency of DNA mismatch repair (9, 11, 14, 36).

## Materials and Methods

Taq MutS was expressed in *E. coli*, purified, and dye labeled at the M88C position as described (21). Taq MutL was cloned from Taq strain YT-1 (ATCC) genomic DNA into expression vectors either with or without His-tags, expressed in *E. coli* and purified by affinity, ion-exchange, and gel-filtration chromatography. A cysteine was inserted between the 6His-tag and MutL sequence for labeling, when indicated. The 550-bp DNA substrates are similar to those described previously (21), except an unintended internal flap overhang was corrected. Lipid passivated, streptavidin surfaces were used to immobilize biotinylated/digoxin-labeled DNA substrates, which could be blocked at the nonsurface tethered end by antidigoxin binding as described previously (21). smFRET was measured in a prism-type total internal reflection fluorescence microscope with a dualview image splitter before an emCCD and analyzed as described previously (21, 37). Experiments to determine complex stoichiometry were performed by mixing biotinylated DNA, ATP, MutS, and MutL in solution 10 min before adding glutaraldehyde to 0.8% final concentration for 1 min, diluting 46-fold with Tris buffer (20 mM Tris·HCl, 100 mM NaOAc, 5 mM $MgCl_2$ pH 7.8) to quench crosslinking, flowing over an imaging surface coated with streptavidin islands and lipid bilayer passivation. This surface captured complexes via biotinylated DNA for single molecule fluorescence imaging and photobleaching step counting. All imaging was performed in imaging buffer (20 mM Tris·acetic acid, pH 7.8, 100 mM NaOAc, 5 mM $MgCl_2$, 2% glucose (wt/wt) with oxygen scavenging/triplet state quenching additives, 100 units/mL glucose oxidase, 1,000 units/mL catalase, 0.05 mg/mL cyclooctatetraene, and 14 mM 2-mercaptoethanol). Additional details are available in *SI Materials and Methods*.

**Note Added in Proof.** A recently published study demonstrated that addition of *E. coli* MutL greatly reduces the rate at which MutS slides off mismatched DNA, consistent with our findings (41).

**ACKNOWLEDGMENTS.** We thank Anushi Sharma for helpful discussions. This work is funded by American Cancer Society Research Scholar Grant RSG-10-048 (to K.R.W.), NIH Grants GM079480 and GM080294 (to D.A.E.) and GM109832 (to D.A.E. and K.R.W.), and GM045190 (to P.M.), and National Science Foundation Grant MCB 1022203 (to M.M.H.). P.M. is an Investigator of the Howard Hughes Medical Institute.

1. Martín-López JV, Fishel R (2013) The mechanism of mismatch repair and the functional analysis of mismatch repair defects in Lynch syndrome. *Fam Cancer* 12(2): 159–168.
2. Rasmussen LJ, et al. (2012) Pathological assessment of mismatch repair gene variants in Lynch syndrome: Past, present, and future. *Hum Mutat* 33(12):1617–1625.
3. Grilley M, Welsh KM, Su SS, Modrich P (1989) Isolation and characterization of the Escherichia coli mutL gene product. *J Biol Chem* 264(2):1000–1004.
4. Habraken Y, Sung P, Prakash L, Prakash S (1998) ATP-dependent assembly of a ternary complex consisting of a DNA mismatch and the yeast MSH2-MSH6 and MLH1-PMS1 protein complexes. *J Biol Chem* 273(16):9837–9841.
5. Erie DA, Weninger KR (2014) Single molecule studies of DNA mismatch repair. *DNA Repair (Amst)* 20:71–81.
6. Iyer RR, Pluciennik A, Burdett V, Modrich PL (2006) DNA mismatch repair: Functions and mechanisms. *Chem Rev* 106(2):302–323.
7. Modrich P (1987) DNA mismatch correction. *Annu Rev Biochem* 56:435–466.
8. Hsieh P, Yamane K (2008) DNA mismatch repair: Molecular mechanism, cancer, and ageing. *Mech Ageing Dev* 129(7-8):391–407.
9. Kadyrov FA, Dzantiev L, Constantin N, Modrich P (2006) Endonucleolytic function of MutLalpha in human mismatch repair. *Cell* 126(2):297–308.
10. Pluciennik A, et al. (2010) PCNA function in the activation and strand direction of MutLα endonuclease in mismatch repair. *Proc Natl Acad Sci USA* 107(37):16066–16071.
11. Kadyrov FA, et al. (2007) Saccharomyces cerevisiae MutLalpha is a mismatch repair endonuclease. *J Biol Chem* 282(51):37181–37190.
12. Pluciennik A, et al. (2013) Extrahelical (CAG)/(CTG) triplet repeat elements support proliferating cell nuclear antigen loading and MutLα endonuclease activation. *Proc Natl Acad Sci USA* 110(30):12277–12282.
13. Deschênes SM, et al. (2007) The E705K mutation in hPMS2 exerts recessive, not dominant, effects on mismatch repair. *Cancer Lett* 249(2):148–156.
14. Pillon MC, et al. (2010) Structure of the endonuclease domain of MutL: Unlicensed to cut. *Mol Cell* 39(1):145–151.
15. Kunkel TA, Erie DA (2005) DNA mismatch repair. *Annu Rev Biochem* 74:681–710.
16. Gorman J, et al. (2012) Single-molecule imaging reveals target-search mechanisms during DNA mismatch repair. *Proc Natl Acad Sci USA* 109(45):E3074–E3083.
17. Gradia S, et al. (1999) hMSH2-hMSH6 forms a hydrolysis-independent sliding clamp on mismatched DNA. *Mol Cell* 3(2):255–261.
18. Hombauer H, Campbell CS, Smith CE, Desai A, Kolodner RD (2011) Visualization of eukaryotic DNA mismatch repair reveals distinct recognition and repair intermediates. *Cell* 147(5):1040–1053.
19. Iaccarino I, Marra G, Dufner P, Jiricny J (2000) Mutation in the magnesium binding site of hMSH6 disables the hMutSalpha sliding clamp from translocating along DNA. *J Biol Chem* 275(3):2080–2086.
20. Jeong C, et al. (2011) MutS switches between two fundamentally distinct clamps during mismatch repair. *Nat Struct Mol Biol* 18(3):379–385.
21. Qiu R, et al. (2012) Large conformational changes in MutS during DNA scanning, mismatch recognition and repair signalling. *EMBO J* 31(11):2528–2540.
22. Elez M, Radman M, Matic I (2012) Stoichiometry of MutS and MutL at unrepaired mismatches in vivo suggests a mechanism of repair. *Nucleic Acids Res* 40(9):3929–3938.
23. Srivatsan A, Bowen N, Kolodner RD (2014) Mispair-specific recruitment of the Mlh1-Pms1 complex identifies repair substrates of the Saccharomyces cerevisiae Msh2-Msh3 complex. *J Biol Chem* 289(13):9352–9364.
24. Acharya S, Foster PL, Brooks P, Fishel R (2003) The coordinated functions of the E. coli MutS and MutL proteins in mismatch repair. *Mol Cell* 12(1):233–246.
25. Schofield MJ, Nayak S, Scott TH, Du C, Hsieh P (2001) Interaction of Escherichia coli MutS and MutL at a DNA mismatch. *J Biol Chem* 276(30):28291–28299.
26. Floyd DL, Harrison SC, van Oijen AM (2010) Analysis of kinetic intermediates in single-particle dwell-time distributions. *Biophys J* 99(2):360–366.
27. Yildiz A, et al. (2003) Myosin V walks hand-over-hand: Single fluorophore imaging with 1.5-nm localization. *Science* 300(5628):2061–2065.
28. Sharma A, Doucette C, Biro FN, Hingorani MM (2013) Slow conformational changes in MutS and DNA direct ordered transitions between mismatch search, recognition and signaling of DNA repair. *J Mol Biol* 425(22):4192–4205.
29. Antony E, Hingorani MM (2004) Asymmetric ATP binding and hydrolysis activity of the Thermus aquaticus MutS dimer is key to modulation of its interactions with mismatched DNA. *Biochemistry* 43(41):13115–13128.
30. Hess MT, Gupta RD, Kolodner RD (2002) Dominant Saccharomyces cerevisiae msh6 mutations cause increased mispair binding and decreased dissociation from mispairs by Msh2-Msh6 in the presence of ATP. *J Biol Chem* 277(28):25545–25553.
31. Hura GL, et al. (2013) DNA conformations in mismatch repair probed in solution by X-ray scattering from gold nanocrystals. *Proc Natl Acad Sci USA* 110(43):17308–17313.
32. DeRocco VC, Sass LE, Qiu R, Weninger KR, Erie DA (2014) Dynamics of MutS-mismatched DNA complexes are predictive of their repair phenotypes. *Biochemistry* 53(12):2043–2052.
33. Wang H, et al. (2003) DNA bending and unbending by MutS govern mismatch recognition and specificity. *Proc Natl Acad Sci USA* 100(25):14822–14827.
34. Pluciennik A, Burdett V, Lukianova O, O'Donnell M, Modrich P (2009) Involvement of the beta clamp in methyl-directed mismatch repair in vitro. *J Biol Chem* 284(47): 32782–32791.
35. Dao V, Modrich P (1998) Mismatch-, MutS-, MutL-, and helicase II-dependent unwinding from the single-strand break of an incised heteroduplex. *J Biol Chem* 273(15): 9202–9207.
36. Pillon MC, Miller JH, Guarné A (2011) The endonuclease domain of MutL interacts with the β sliding clamp. *DNA Repair (Amst)* 10(1):87–93.
37. Sass LE, Lanyi C, Weninger K, Erie DA (2010) Single-molecule FRET TACKLE reveals highly dynamic mismatched DNA-MutS complexes. *Biochemistry* 49(14):3174–3190.
38. Jacobs-Palmer E, Hingorani MM (2007) The effects of nucleotides on MutS-DNA binding kinetics clarify the role of MutS ATPase activity in mismatch repair. *J Mol Biol* 366(4):1087–1098.
39. Mendillo ML, Mazur DJ, Kolodner RD (2005) Analysis of the interaction between the Saccharomyces cerevisiae MSH2-MSH6 and MLH1-PMS1 complexes with DNA using a reversible DNA end-blocking system. *J Biol Chem* 280(23):22245–22257.
40. Yang Y, Wang H, Erie DA (2003) Quantitative characterization of biomolecular assemblies and interactions using atomic force microscopy. *Methods* 29(2):175–187.
41. Groothuizen FS, et al. (2015) MutS/MutL crystal structure reveals that MutS sliding clamp loads MutL onto DNA. *Elife*, 10.7554/eLife.06744.